Arctic Stratus Cloud Properties and Radiative Forcing Derived From Ground-based Data Collected at Barrow, Alaska

Xiquan Dong and Gerald G. Mace, University of Utah

Corresponding author address: Dr. Xiquan Dong, Meteorology Department, University of Utah, 135 S. 1460 E. Rm 819, Salt Lake City, UT 84112. Email: xdong@met.utah.edu

Abstract: A record of single-layer and overcast low-level Arctic stratus cloud properties has been generated using data collected at the Atmospheric Radiation Measurement site near Barrow, Alaska from May to September 2000. The record includes liquid-phase and liquid dominant mixed-phase Arctic stratus macrophysical, microphysical, and radiative properties, as well as surface radiation budget and cloud radiative forcing. The macrophysical properties consist of cloud fractions, base/top heights and temperatures, and cloud thickness derived from a ground-based radar and lidar pair, and rawinsonde sounding. The microphysical properties include cloud liquid water path and content, and cloud-droplet effective radius and number concentration obtained from microwave radiometer brightness temperature measurements, and a newly developed parameterization. The radiative properties contain cloud optical depth, effective solar transmission, and surface/cloud/top-of-atmosphere albedos derived from a newly developed parameterization and standard Epply precision spectral pyranometers. The shortwave, longwave, and net cloud radiative forcings at the surface are inferred from the measurements of standard Epply precision spectral pyranometers and pyrgeometers. There are approximately 300 hours and more than 3600 samples (5-min resolution) of single-layer and overcast low-level stratus during the study period. The 10-day averaged total and low cloud (Z_{top} < 3 km) occurrence fractions vary from 0.7 to 1.0 and from 0.4 to 0.8, with the mean values of 0.87 and 0.55, respectively. The 10-day averaged low cloud base heights are, in general, around 0.4 km, and top heights around 0.8 km, leading to 0.4 km of cloud thickness. During the spring season, the effective radius and number concentration are found to be 8 μm and 220 cm^{-3} - similar to the microphysical properties of midlatitudes continental stratus clouds. The means of cloud-droplet effective radius and number concentration are around 13 μm and 60 cm^{-3} during the summer - similar to the microphysical properties of midlatitudes marine stratus. These cloud macrophysical and microphysical properties when compared statistically with FIRE ACE and SHEBA data sets can approximately represent a climatology of Arctic stratus cloud properties during May-September period. Comparing the net CRFs at the ARM NSA site with those at the SHEBA ship, the summer cooling period at the NSA site is much longer (2-3 months vs. 1-2 weeks), and the values of negative net CRF are much larger (-100 W m^{-2} vs. -5 W m^{-2}).

1. Introduction

Clouds are the dominant modulators of radiation in the Arctic both at the surface and top of atmosphere. Their impact on the radiation fluxes depends on cloud particle size and shape, and the amount and phase of condensed water and its vertical and horizontal distributions (Curry et al. 2000; Randall et al. 1998). The cloud-radiative interactions in the Arctic are very complex due to low temperatures and humidity, large solar zenith angles, the presence of the highly reflective and inhomogeneous snow/ice surfaces and multiple cloud layers, and persistent temperature inversions (Curry et al. 1996; Stamnes et al. 1999). The importance of cloud-radiative interactions to global climate has been highlighted by many investigators (e.g., Wetherald and Manabe 1988; Mitchell and Ingram 1992) and recent climate modeling results have revealed that the largest disagreement between coupled climate model simulations of present-day climate is found in the Arctic region (Gates et al. 1996; Tao et al. 1996). These results reflect the weakness of our current understanding of the sensitivity of the simulated Arctic climate to different formulations of various physical processes in global models (Randall et al. 1998). An aspect of Arctic clouds that makes them difficult to treat in climate models is that they are often optically thin, so that their emissivities are often less than one and a function of particle size. The albedo of snow has a strong spectral variation and a function of the ratio of direct-to-diffuse radiation, both of which are affected by cloud depth, further complicates the treatment of radiative transfer in the cloudy Arctic (reference ?).

To provide a much-needed source of high latitude data concerning the physical state of the Artic atmosphere, several extensive field programs have been conducted in the past several years. The Department of Energy (DOE) Atmospheric Radiation Measurement (ARM) program (Stokes and Scheartz 1994) established the ARM North Slope of Alaska-Adjacent Arctic Ocean (NSA-AAO) site (71.3^{o}N, 156.6^{o}W) at Barrow, Alaska in 1998 (Stamnes et al. 1999). The general approach adopted by the ARM program is to use long records of surface observations to develop, test, and improve cloud parameterizations in the context of single GCM grid columns and then to transfer the resulting parameterizations into full three-dimensional GCMs (Randall et al. 1996). As a precursor to the establishment of the site at Barrow, the ARM program operated concurrently with the First ISCCP (International Satellite Cloud Climatology Project) Regional Experiment (FIRE) Arctic Cloud Experiment (ACE) (Curry et al. 2000) and the Surface Heat Budget of the

Arctic Ocean (SHEBA) project (Perovich et al. 1999). In addition to observations collected at Barrow, ARM surface-based instruments were also installed on or near the SHEBA ship that served as a floating science station and drifted from 75.3°N, 142.7°W to 80.5°N, 166°W during October 1997-October 1998, FIRE ACE were to make aircraft observations and satellite retrievals over the SHEBA ship (~77°N, 165°W) and Barrow from April to July 1998 (Curry et al. 2000). ARM, FIRE, and SHEBA share scientific objectives that focus on collecting and evaluating data so that the physical processes that drive the large-scale atmosphere in the Artic are more faithfully represented (Randall et al. 1998). In particular, ARM is a long-term program (~10 years) of surface-based observations and modeling of clouds and radiation at Barrow, FIRE ACE was to improve the satellite retrieval of cloud and surface characteristics in the Arctic using aircraft in situ measurements during the 4-month period, while SHEBA was a one-year observational program to emphasize the surface energy balance and the sea ice mass balance of the Arctic ocean (Curry et al. 2000; Randall et al. 1998).

To begin the process of evaluating cloud parameterizations and validating satellite retrievals using data collected at Barrow, we have compiled a 5-month record of single-layer and overcast low-level stratus cloud macrophysical, microphysical, and radiative properties, as well as surface radiation budget and cloud radiative forcing using data collected at the ARM NSA site near Barrow, Alaska from May to September 2000 (referred to collectively as the summer 2000 results). During this period, the liquid-phase and liquid dominant mixed-phase low-level Arctic stratus clouds occurred frequently, which makes it possible to retrieve their microphysical and radiative properties using the newly developed parameterization. The record of cloud properties provides a unique source of information for studying the seasonal variation of Arctic stratus cloud properties and their impact on the surface radiation budget. In order to establish the representativeness of the data sets collected at Barrow during summer 2000, the cloud properties are compared with similar properties derived from aircraft in situ measurements (Lawson et al. 2001; Hobbs et al. 2001; Dong et al. 2001), surface observations (Intrieri et al. 2001 a & b; Curry et al. 2001), and satellite data (Minnis et al. 2001; Maslanik et al. 2001) during the FIRE ACE and SHEBA field experiments. We also compare the summer 2000 results with the aircraft in situ measurements collected over the Beaufort Sea during the Arctic Stratus Clouds (ASC) experiment in June 1980 (Herman and Curry 1984; Tsay and Jayaweera 1984) and the Beaufort

and Arctic Storms Experiment (BASE) in autumn 1994 (Pinto et al. 2001), as well as from Hobb and Rangno's study in June 1995 (Hobbs and Rangno 1998). Although these comparisons are based on data collected at different locations and different years (the same months), this allows us to pose the following scientific questions:

1) What are the seasonal variation of Arctic stratus cloud macrophysical, microphysical, and radiative properties at Barrow, Alaska from spring to autumn? and how does this seasonal variation of cloud properties influence the surface radiation budget, cooling or warming, and when?
2) How do the summer 2000 results, generated at a single point over one summer, represent the Arctic summer climatology? For example, what are the differences between the cloud properties and associated radiative forcing found in data sets collected at Barrow and the SHEBA ship? Is the summer cloud cooling effect at Barrow longer and stronger than at the SHEBA ship?

2. Data

The data sets in this study are collected from direct surface measurements or derived from surface measurements, as well as calculated from a newly developed parameterization (see the appendix). The main surface observations at the ARM NSA-AAO site in this study are listed in Table 1. The millimeter wavelength cloud radar (MMCR; Moran et al. 1998) is the centerpiece of this instrument array. The MMCR operates at a wavelength of 8 mm in a vertically pointing mode, and provides continuous profiles of radar reflectivity from hydrometers advecting through the radar field of view allowing us to identify clear and cloudy conditions. The cloud top height (Z_{top}) is derived from MMCR reflectivity profile, and cloud base height (Z_{base}) is derived from the laser ceilometer. Since the laser ceilometer is sensitive to the 2nd moment of the particle distribution instead of the 6th like the MMCR, the ceilometer provides a more faithful estimate of cloud base. The temporal and vertical resolutions and maximum detected heights of MMCR and ceilometer are listed in Table 1. The total and low cloud fractions are calculated for a specified time period (10 days in this study) from the combined measurements of MMCR and ceilometer as the fraction of time that the upward looking narrow field-of-view radar and ceilometer detected clouds. The total cloud fraction is the fraction of time cloud detected anywhere in the vertical column and the low cloud fraction is the fraction of time low (Z_{top} < 3km) cloud detected

during the 10-day period. Values of cloud base and top temperatures (T_{base} and T_{top}) are found from the ARM NSA rawinsonde sounding (once per day at around local noon) using Z_{base} and Z_{top} derived from the ceilometer and radar data.

The cloud liquid water path (LWP) is derived from the microwave radiometer brightness temperatures measured at 23.8 and 31.4 GHz using a statistical retrieval method (Liljegren et al. 2001). The root-mean-square (RMS) accuracies of the retrievals are about 20 g m^{-2} and 10% for cloud LWP below and above 200 g m^{-2}, respectively (Dong et al. 2000, hereafter D00; Liljegren et al. 2001). This retrieval method may overestimate the LWP of supercooled clouds (Westwater et al. 2001) due to poorly known absorption coefficients and an incorrect treatment of the cloud liquid dielectric model. However, the overestimation of LWP (~10-20 g m^{-2}) is within the expected accuracy of the retrievals (Liljegren, personal communication, 2001), and its influence on the retrieved effective radius is also within the uncertainty of retrieved effective radius (Dong et al. 1997, 1998, hereafter D97, D98). Therefore, the low limit of LWP is set to 20 g m^{-2} and the original LWP retrievals are used in this study.

The up- and down-looking standard Eppley Precision Spectral Pyranometers (PSPs) and Precision Infrared Pyrgeometers (PIRs) provide measurements of downward and upward broadband shortwave (0.3 to 3 μm) and longwave (4-50 μm) fluxes at the surface, respectively. The absolute accuracies of PSP and PIR measurements are approximately 10 Wm^{-2} (Long and Ackerman 2000). The surface albedo (R_{sfc}) is derived from the ratio of upward to downward shortwave flux measurements. The effective solar transmission (γ) is the ratio of the measured cloudy downward shortwave flux at the surface to the inferred clear-sky downward shortwave flux that would be recorded by the broadband pyranometer if there were no clouds. Long and Ackerman (2000) first fit the downward shortwave flux measurements on the clear-sky days that are closest in time to the cloudy days, and then interpolate the empirical curve-fitting values to cloudy days to estimate clear-sky downward shortwave fluxes that would be observed under the assumption of constant aerosol optical depth during this time period. The aerosol optical depth can vary by a factor of 4 over a short period of time during Arctic Haze events (which are common in spring) when aerosol optical depth can be as high as 0.5 (e.g., Stone 2001). These variations may have a significant impact on the inferred clear-sky shortwave flux and thus affect

the retrievals of cloud property. Strictly speaking, the inferred clear-sky downward shortwave fluxes on the cloudy days are not measurements; nonetheless, they are derived from the measurements and should be more appropriate than model calculations in estimation of γ because the estimated clear-sky values automatically incorporate any biases between measured and modeled surface downward shortwave fluxes (Kato et al. 1997). The γ increases with increased R_{sfc} because the PSP-measured cloudy downward solar flux at the surface includes the multiple reflections of solar radiation between the cloud layer and the highly reflective surface (see Fig. A1 of the appendix).

The cloud-droplet effective radius (r_e), number concentration (N), broadband shortwave optical depth (τ), and bulk albedos at the top of cloud and atmosphere (R_{cldy}, R_{TOA}) with the underlying reflecting surface are calculated by a newly developed parameterization (see the appendix). The new parameterization is the same as that described by D98 except the impact of surface albedo is included. More details about the retrieval method and old/new parameterizations are discussed in the appendix. The uncertainties in τ, R_{cldy}, and R_{TOA} are generally less than 5%, while in r_e and N they are about 10 and 30%, respectively (D97, D98).

3. Results

We have established five criteria for choosing the conditions under which cloud properties are estimated using the new parameterization. These criteria are (i) only single-layer low-level stratiform clouds are present as determined from cloud radar observations, (ii) the cosine of solar zenith angle (μ_0) is larger than 0.2, (iii) the range of γ is between 0.1 and 0.8, (iv) LWP is between 20 and 600 gm^{-2}, and (v) Z_{top} is less than 3 km. The physical reasons for using these five criteria are discussed in D00. We identified approximately 300 hours (more than 3600 samples at 5-min resolution) that satisfied these five criteria during the study period. The observed and derived 300 hours of elements include cloud base/top heights (Z_{base}/Z_{top}) and temperatures (T_{base}/T_{top}), cloud-layer geometric thickness (ΔZ), cloud LWP and LWC, cloud-droplet effective radius (r_e) and number concentration (N), broadband shortwave optical thickness depth (τ), effective solar transmission (γ), surface albedo (R_{sfc}) with a cloud above, bulk albedos at the top of cloud and atmosphere (R_{cldy}, R_{TOA}) with the underlying reflecting surface, and cloudy net

shortwave (SW) and longwave (LW) fluxes. Other elements, including total and low cloud fractions (C_{tot}, C_{low}) and clear-sky net SW and LW fluxes, are compiled irrespective of the five conditions listed above.

With limited samples during the 10-day period, the clear-sky LW mean flux can provide a reasonable value because LW flux does not change too much for the daytime, but SW flux is strongly dependent on solar zenith angle and cannot represent real clear-sky information. Therefore, we use the empirical curve-fitting technique to infer clear-sky downward SW flux, and then use it with all-sky (clear and cloudy) measured R_{sfc} to infer clear-sky upward SW flux. We note that all-sky R_{sfc} is slightly different from clear-sky R_{sfc}, but this appears to be the most reasonable approach to inferring the clear-sky SW fluxes for conditions that are predominantly cloudy. The clear-sky net LW and SW fluxes are deduced from the difference between downward and upward fluxes for $\mu_0>0.2$ during the 10-day period to be consistent with the cloudy net fluxes. The clear-sky values are then used to derive LW and SW cloud forcing. The 10-day means of the various elements (except the cloud occurrence fractions) are compiled from the periods that satisfied the five criteria during the 10-day period.

a. Macrophysical properties

The 10-day means and standard deviations of cloud macrophysical properties from May to September 2000 at the ARM NSA site are shown in Fig. 1, and the corresponding frequency distributions during the 5-month period are shown in Fig. 2. These means (so do standard deviations and frequency distributions) are simply the averages of total and low cloud occurrences for all cloudy conditions, and the averages of the selected samples (5-min temporal resolution) using five criteria for cloud base and top heights/temperatures (so do other cloud parameters) within a 10-day period. The averaged C_{tot} during the 5-month study period is 0.87 with a maximum of 0.96 in September and a minimum of 0.77 in June, and the averaged C_{low} is 0.55 with a maximum of 0.69 in May and a minimum of 0.47 in June. From high values of total and low cloud fractions, we can draw a conclusion that the ARM NSA site is an ideal site to study clouds, especially low-level stratus clouds. The 10-day averaged Z_{base} and Z_{top} altitudes are, in general, around 0.4 and 0.8 km, leading to a ΔZ of 0.4 km. From the frequency distributions, most Z_{base} values are less than 1 km with a mean value of 0.47 km and a standard deviation of

0.56 km, and most Z_{top} values are less than 1.5 km and have a broad frequency of occurrence histogram. Most T_{base} and T_{top} values are above 0 ^{o}C from late June to early September, whereas others range from –10 ^{o}C to 0 ^{o}C with liquid dominant mixed-phase stratus clouds.

b. Microphysical properties

The 10-day means and standard deviations of cloud microphysical properties are shown in Fig. 3, and the corresponding frequency distributions are also shown in Fig. 2. Most 10-day averaged cloud LWPs range from 50 to 150 g m^{-2}, and more than 85% of the cloud LWPs are less than 150 g m^{-2} with mean and standard deviation of 91 and 67 g m^{-2}, respectively. Cloud LWC is the ratio of cloud LWP to ΔZ. The 10-day means of cloud LWC increase from early May (0.2 g m^{-3}) to the summer (0.35 g m^{-3}), then decrease to 0.2 g m^{-3} in late September. Thus, cloud LWC during this summer period at the NSA site increases with increased cloud temperature. This positive correlation (0.31) between LWC and cloud temperature is not found using data collected at the ARM Southern Great Plains (SGP) site (36.6^{o}N, 97.5^{o}W) (D00). We find no correlation between cloud LWP and cloud temperature in this study nor are this correlation found at the ARM SGP site (Table 2 in D00). These findings are based on 10-day means in this study and monthly means at the ARM SGP site; it may be unreliable to draw conclusions from comparison of time series of 10-day or monthly means. The only difference between these two quantities (LWP and LWC) is the cloud geometric thickness. This suggests that warmer clouds are thinner but contain higher LWCs than cold ones, which is only true at the ARM NSA site, not at the ARM SGP site. The difference in the relationships between cloud thickness and temperature at the NSA and SGP sites may reveal that the formation, maintenance, and dissipation processes of stratus clouds in the midlatitudes and Arctic are different. Preliminary calculations suggest these correlations are substantially low at higher temporal resolution and additional study is ongoing to explain these findings.

The 10-day means and standard deviations of r_e and N are illustrated in Fig. 3, and their frequency distributions are also shown in Fig. 2. The means of r_e monotonically increase from early May to mid June, then begin to decrease in August. Overall, r_e is larger during the summer than in the spring and autumn. As Fig. 2 demonstrates, most effective radii range from 4 to 16 μm with a bimodal distribution. The small and large modes appear to peak at 6-7 μm and 11-14

μm, respectively. The former is mainly consisted of clouds that were observed during the spring and autumn, while the later is mostly from clouds observed during the summer. The variation of N is always complementary to that of r_e with much smaller values during the summer than in the spring and autumn (Fig. 3). More than 70% of N values are less than 150 cm^{-3} with a mean and standard deviation of 117 and 113 cm^{-3}, respectively. During the summer, the means of r_e and N are around 13 μm and 60 cm^{-3}, which are the same as the midlatitudes marine stratus cloud microphysics (D97). While during the spring and autumn seasons, the means of r_e vary from 7 to 10 μm, and the N values are around 200 cm^{-3} - very similar to the midlatitudes continental stratus cloud microphysics (D97; D98; D00; Dong et al. 2002).

We note that the variations of r_e and N in this study are almost the same as that reported in D00 using data collected at the ARM SGP site. This suggests that similar seasonally varying factors may be influencing the cloud microphysical properties at the two sites. These factors include the increased levels of absolute humidity in the warmer temperatures, more vigorous boundary layer dynamics due to solar heating, and/or a decrease in the strength of the inversion near cloud top. Aerosol effects may be another factor for the variation of cloud microphysics at the NSA site as we discussed in Section 2. All factors that may lead to the seasonal variation of cloud microphysics are discussed in next section. We now demonstrate how this seasonal cycle in cloud microphysics influences the seasonal variation of cloud radiative properties.

c. Radiative properties

The calculated broadband cloud optical thickness (τ), and bulk albedos at the top of cloud and atmosphere (R_{cldy}, R_{TOA}), as well as PSP-derived effective solar transmission (γ) and surface albedo (R_{sfc}) are illustrated in Fig. 4, and their frequency distributions are shown in Fig. 5. The R_{sfc} values in May are more than 0.8, then decrease significantly from the beginning to the end of June, and keep nearly a constant value of 0.16 for the whole summer, and finally increase from early to late September (0.8). The large standard deviation of R_{sfc} in mid June suggests that snow melted quickly in that time period, while the first snow of the coming winter occurred in the middle of September. We have noted that cloudy-sky albedo of snow is approximately 5% higher than the clear-sky albedo of snow because snow reflects diffuse solar radiation better than

direct solar radiation and clouds attenuate near-IR radiation more efficiently than visible radiation.

The variations of the 10-day means of R_{cldy} and R_{TOA} basically follow the trend of R_{sfc}. These results confirm that R_{cldy} and R_{TOA} depend on both τ and R_{sfc}. During summer R_{cldy} and R_{TOA} are mainly determined by τ, and don't depend on R_{sfc} because R_{sfc} is low and constant. As Fig. A1 (see the appendix) demonstrates, the dependence of R_{cldy} on τ becomes less and less with the increased R_{sfc} for non-absorption cloud. This argument has been confirmed by the R_{cldy} values in mid and late September periods where τ is smaller and R_{cldy} and R_{sfc} are larger in late September than in mid September. The variation in the 10-day means of τ follows the variation of LWP, and most of τ values are between 5 and 20 with a mean value of 12.9 (Fig. 5). Only 6% of τ values are less than 5, which are mainly due to the criteria (iii) and (iv) listed in the beginning of this Section. γ is negatively correlated to τ for low R_{sfc}, but this correlation is significantly modified under the snow/ice-covered surface. For instance, the τ (~15) in early June is almost double the value (~8) in mid June, whereas, the γ values in these two periods are nearly the same. This is mainly due to the R_{sfc} difference where the former R_{sfc} (0.74) is about 50% higher than latter R_{sfc} (0.49). The higher R_{sfc} leads to increase the multiple reflections of solar radiation between the cloud layer and the highly reflecting surface, which ultimately results in higher γ.

The importance of r_e and R_{sfc} to R_{cldy} has been demonstrated in Fig. A2 (see the appendix). For fixed LWP, R_{cldy} has a significant dependence on both r_e and R_{sfc}. The seasonal variation of cloud microphysics, small (large) r_e (N) during the spring and large (small) r_e (N) during the summer in this study, strongly supports the seasonal variation of R_{cld} (high in spring and low in summer). We are certain that R_{cldy} is significantly affected by the cloud properties during the summer (low R_{sfc}), but not during the spring because R_{cldy} is insensitive to cloud optical depth when R_{sfc} is high (Fig. A1 and A2).

d. Cloud radiative forcing

The change in the radiation balance due to clouds is termed cloud radiative forcing (CRF). The CRF is classified into shortwave (C_{SW}) and longwave (C_{LW}) CRF and defined as (Ramanathan et al. 1989; Curry et al. 1996)

$$\begin{aligned} C_{SW} &= Q(A_C) - Q(0) \\ C_{LW} &= F(A_C) - F(0), \end{aligned} \tag{1}$$

where A_c is the cloud fraction (A_c=1 in this study), and $Q(A_c)$ and $F(A_c)$ are the net (downward minus upward) SW and LW fluxes during cloudy condition, respectively, while $Q(0)$ and $F(0)$ for clear sky. The net CRF, C_{NET}, is the sum of C_{SW} and C_{LW} at the surface. The values of CRF are positive for warming of the surface and negative for cooling of the surface.

The cloudy and clear-sky net SW and LW fluxes, and SW/LW/NET CRFs are shown in Fig. 6, where the filled circles represent the averaged cloudy net SW and LW fluxes in a 10-day period, and open circles represent the averaged clear-sky net SW and LW fluxes in that period in the two upper panels of Fig. 6. As Fig. 6 demonstrates, both cloudy and clear-sky net SW fluxes are relatively small (~50 W m^{-2}), and clear-sky net SW flux is only slightly higher than cloudy net SW flux when R_{sfc} is high. However, during the summer when R_{sfc} is low, both cloudy (~100-200 W m^{-2}) and clear-sky (~300-400 W m^{-2}) net SW fluxes are large with a peak during late June-early July, and clear-sky net SW flux is much larger than cloudy net SW flux showing that the SW cooling effect of Arctic stratus is obvious and dominant during the summer at the NSA site. The cloudy net LW flux is nearly flat and around -20 W m^{-2} during the study period because the cloud base temperature is nearly the same as surface temperature at the NSA site where cloud bases are very low and the surface tends to be very wet so that any surplus energy is used in evaporation instead of heating. The clear-sky net LW flux decreases approximately from –50 W m^{-2} in May to –100 W m^{-2} in July due to the significant increase of surface temperature from May to July that results in increasing upward LW flux.

Compared to the SW CRFs, the LW CRFs maintain relatively small positive values and vary slightly during the 5-month period. The LW CRFs range from around 40 W m^{-2} in May to 70 W m^{-2} during July-August, while the SW CRFs vary from –30 W m^{-2} in May to –170 W m^{-2} during July-August, and then return in September. The net CRFs drop from a small positive value (~10 W m^{-2}) in May to a large negative value (–100 W m^{-2}) in the summer, and then return in

September. The variation of net CRFs is mainly determined by the SW CRFs and the trend of net CRF variation is nearly the same as that of R_{sfc} except during the middle of July. During the summer, R_{sfc} is low and net CRF values are large but negative – a strong cooling effect that is the same as low and middle latitudes stratus clouds (Ramanathan et al. 1989; Harrison et al. 1990; Hartmann et al. 1992). During the spring and autumn seasons, the SW CRFs are small and the LW CRFs are the dominant factor in the net CRFs. The positive net CRFs during the spring and autumn seasons suggest that Arctic stratus clouds have a warming effect on the surface, which may enhance the melting of the ice during the spring and slow down the freezing of the ice pack during the autumn relative to a cloudless atmosphere.

Understanding the impact of cloud properties on the surface energy balance is not always straightforward, however. For example, all net CRFs (Fig. 6) during the summer are around –100 W m^{-2} except the middle of July. During the summer, all τ values are more than or around 10 except the middle of July (~6) that allows some of the direct solar flux to penetrate clouds to the surface. Therefore, the SW CRF has a small negative value and results in a small negative net CRF in mid July. The reason leading to the bump of net CRF in mid July is mainly due to our criterion (iii) where the range of γ is between 0.1 and 0.8 in this study. In all previous studies, the maximum of γ was set to 0.7 ensuring that only diffuse solar radiation was recorded by the ground-based solar radiometers. The maximum of 0.8 in this study is reasonable to account for the multiple reflections of solar radiation between the cloud layer and the highly reflective snow/ice surface, which the diffuse solar transmission is still dominant. However, for lower R_{sfc} during summer, the maximum of 0.8 is slightly high and results in including some situations where direct solar flux contributes to the ground-based PSP observations. The apparent anomaly in the middle of July includes a significant number of such cases. If we set the maximum of γ to 0.7, the new net CRF will be –96 Wm^{-2} for that period, which is much higher than the old value (-52 Wm^{-2}) and also much closer to the net CRFs of nearby time periods. This new set (γ_{max}=0.7) significantly affects the net CRF calculation in mid July but not for other time periods because the percentage of γ>0.7 is more than 35% for mid July, while is less than 5% for other 10-day periods during the summer.

The bump of net CRF in mid July also suggests that there are other factors affecting net CRF except R_{sfc}, and motivates us to calculate the correlation coefficients between net CRF and cloud parameters. The correlation coefficients between net CRF and R_{sfc}, γ, and τ from the averages of 15 10-day periods in this study are 0.79, 0.53, and –0.24, respectively. It is easy for us to understand the positive correlation between net CRF and R_{sfc} because net CRF values are small positive for high R_{sfc} and large negative for low R_{sfc}. The positive (negative) correlation between net CRF and γ (τ) is also understandable because a low (large) solar transmission (optical depth) will result in a small cloudy net SW flux and a large negative net SW CRF, and therefore a large negative net CRF. A more complete understanding of the quantitative correlations between the SW/LW/Net CRFs and the cloud parameters should be determined from higher temporal resolution data, such as hourly or daily, rather than 10-day averages and by examining the meteorological situations that contribute to the formation and maintenance of cloud fields in this region.

e. Summary

The single-layer and overcast low-level Arctic stratus macrophysical, microphysical, and radiative properties, as well as surface radiation budget and cloud radiative forcing at the ARM NSA site are summarized as a function of month in Table 2. Both C_{low} and C_{tot} have a minimum in June and their maximums are in May and September, respectively. Most values of Z_{base} are around 0.4 km and Z_{top} are 0.8 km except in September where both Z_{base} and Z_{top} values are more than 1 km. Both T_{base} and T_{top} increase more than 10 K from the spring to the summer where the Arctic stratus has changed from liquid dominant mixed phase to liquid phase only. The r_e and N values in the spring are very similar to the midlatitudes continental stratus cloud microphysics (D00), and in the summer they are very similar to the midlatitudes marine stratus cloud microphysics (D97). R_{cldy} and γ depend on both τ and R_{sfc} when R_{sfc} is high. If we define the seasons at the ARM NSA site based on this study, from May to mid June is the transition season of spring melting, during late June-early September is summer, while the transition season of autumn freezing starts at mid September. During the summer, Arctic stratus clouds have a strong cooling effect on the surface while during the spring and autumn seasons, they have a slight warming effect at the ARM NSA site.

4. Discussion and comparisons with other data sets

To determine how well the data collected at Barrow and analyzed in this study represent cloud properties in the Western Arctic region, it is necessary to compare with other field observations. Therefore, we compare the summer 2000 results with aircraft in situ measurements (Lawson et al. 2001; Hobbs et al. 2001; Dong et al. 2001), surface observations (Intrieri et al. 2001 a&b; Curry et al. 2001), and satellite retrievals (Minnis et al. 2001; Maslanik et al. 2001) during the FIRE ACE and SHEBA experiments. We also compare with aircraft in situ measurements collected over the Beaufort Sea during the Arctic Stratus Clouds (ASC) experiment in June 1980 (Herman and Curry 1984; Tsay and Jayaweera 1984) and the Beaufort and Arctic Storms Experiment (BASE) in autumn 1994 (Pinto et al. 2001), as well as from Hobb and Rangno's study in June 1995 (Hobbs and Rangno 1998). Although these comparisons are based on the data collected at different locations and years, it will be instructive to consider the similarities and differences between the ARM NSA results and data collected in these other field campaigns.

a. Cloud formation, maintenance, and dissipation processes

A strong temperature inversion at the top of boundary layer due to the large-scale subsidence combined with sea-surface cooling plays a central role in the formation of marine stratiform cloud layers (Lilly 1968). These stratiform clouds are maintained by vertical mixing, primarily due to the strong radiative cooling at cloud top that promotes cloud growth by cooling the boundary layer and generating turbulence to maintain an upward moisture flux, and the cloud base altitude should equal to the lifting condensation level of the surface air if the vertical mixing is complete (Paluch and Lenschow 1991). However, entrainment at cloud top brings warm dry air from above the inversion into the boundary layer that can evaporate small cloud droplets near cloud top. These two competing processes coexist inside boundary layer clouds, and horizontal inhomogeneities in the cloud layer may be formed if one process is dominant over the other (Paluch and Lenschow 1991). Therefore, Paluch and Lenschow (1991), based on aircraft in situ measurements, developed a conceptual model of the life cycle of a marine stratus layer in the midlatitudes. It starts initially as a thin, homogenous layer, then grows and becomes patchy with time and produces precipitation. This stage is followed by the formation of small cumuli below and eventually disintegrates, leaving a field of cumuli behind.

The summer stratus clouds at the ARM Southern Great Plains (SGP) site (36.6°N, 97.5°W), based on the 25-month data sets in D00, normally form in the morning and dissipate in the afternoon due to strong solar heating at the surface, and whole cloud-layer altitude rises from morning to afternoon. The life cycle of a stratus cloud layer at the ARM SGP site is similar to the conceptual model generated by Paluch and Lenschow (1991) except it is normally dissipated at the end of the cycle instead of producing precipitation. The summer Arctic stratus clouds events at the ARM NSA site, however, tend to last at least a few days, and even more than 10 days in this study. It is apparent that the formation, maintenance, and dissipation processes of stratus clouds in the midlatitudes and the Arctic are significantly different from what typically occurs at SGP or was hypothesized in the conceptual models. Arctic stratus clouds are formed very near the sea-ice surface if warm moist air advects over the cold Arctic Ocean, or by a convective-type process if cold polar air flows over a warmer sea-ice surface (Tsay and Jayaweera, 1984). As Herman and Goody (1976) pointed out that once Arctic stratus clouds form, they persist. This is the significant difference between the Arctic and midlatitudes stratus clouds. In the Arctic the dissipative mechanisms found in the midlatitudes such as precipitation, convective heating from the surface, absorption of solar radiation, and destruction by synoptic activity are either nonexistent or relatively weak. The persistence of the cloud field occurs in a steady state situation where dissipative processes are balanced by advection of air masses into the region and the maintenance of synoptic regimes that are suitable for cloud formation. Certainly further study is required to more fully understand these feedbacks and eventually parameterize these processes in large-scale models.

b. Cloud fraction

The monthly-averaged total cloud fractions derived from this study and during the FIRE ACE and SHEBA experiments are listed in Table 3. The SHEBA radar and lidar derived cloud fraction is defined as the percentage of time that either the radar or lidar observed cloud over the SHEBA ship (Intrieri et al. 2001b). The monthly-averaged cloud fractions from the surface observers are based on 6-hourly visual observations (Minnis et al. 2001; Maslanik et al. 2001). The cloud fractions derived from NOAA-12 and NOAA-14 advanced very high resolution radiometer (AVHRR) High-Resolution Picture Transmission (HRPT) 1-km images in Minnis's study are averaged over the Arctic Ocean for a circular area 25 km in radius centered on the

SHEBA ship. These two satellites provide good diurnal sampling except between 1800-2400 LT (Minnis et al. 2001). The cloud fractions derived from Maslanik's study are based the newly available AVHRR-based Polar Pathfinder (APP) products at a 5-km resolution on 1400 LT for the 105 x 105 km^2 region centered on the SHEBA ship (Maslanik et al. 2001), while those from ISCCP D2 data are averaged for the 72.5^o - 80^{o}N and 130^o - 170^{o}W region from 1983 to 1994 (Minnis et al. 2001).

It is noted that the monthly-averaged cloud fractions derived from the SHEBA radar/lidar pair are generally higher than those derived from the ARM NSA radar/ceilometer pair. This difference may be partially real owing to differences in location and year (surface types, air masses, annual variability, etc.) and partially an artifact of different sampling. The definition of cloud fraction is the same in both studies, the percentage of time clouds over the surface site. However, the cloud fraction is calculated when the clouds are observed by both radar and ceilometer in this study, while by either radar or lidar in Intrieri et al. (2001b). Some of optically thin clouds may be too thin to be detected by radar but have been detected by lidar due to the different sensitivities of radar and lidar to clouds. Radar is sensitive to low density of large drops and lidar is sensitive to high density of small droplets (D97; Intrieri et al. 2001b). Thus, the cloud fractions in this study may be underestimated. However, given the good agreement between this study and SHEBA surface observations and AVHRR results from Minnis's study, it is very difficult to ascertain the cause of this underestimation. The difference of cloud fraction between Minnis and Maslanik's studies is probably due to the following reasons: (i) retrieving technique, (ii) temporal sampling (0000-1800 LT vs. 1400 LT), and (iii) spatial sampling (a 25-km radius vs. 105 x 105 km^2). Despite the scale differences between surface and satellite observations, the limited resolution of the satellite imager pixels, and the low resolution of surface cloud fraction digitization (octas) and surface observer subjectivity, the comparison of cloud fractions between this study and FIRE ACE and SHEBA experiments agree well except from ISCCP D2 data that are approximately 20-30% lower than all other estimates of cloud amount. Overall, the good agreement between SHEBA in 1998 and ARM NSA from summer 2000 has shown that the monthly-averaged total cloud fractions observed during the two field programs are very similar to one another.

c. The climatology of aerosol characteristics and their trajectories

Bigg (1980) reported the aerosol characteristics using data collected at Barrow: (i) sulfuric acid was the dominant winter aerosol and winter size distributions were remarkably constant during 1976-1977; (ii) in spring the sulfuric acid particles were more numerous and larger than in winter and contained a much greater proportion of ammonium sulfate than in winter. In general, the aerosol concentration during January-April is at a maximum and mostly relates to man-made pollutants, between May and June is a second peak due to the increased phytoplankton activity, while in late summer and early autumn is at a minimum due to efficient scavenging by precipitation during the summer months (Pinto et al. 2001; Barrie 1986). Harris and Kahl (1994) used a newly developed isentropic air trajectory model to produce 10-day back trajectories that arrived at near-surface altitudes above Barrow during 1985-1992. They found that the atmospheric flow patterns for the period 1985-1992 depicted by cluster-mean back trajectories arriving at Barrow were mostly southerly/ southwesterly and northeasterly flow during summer and westerly flow during winter. The former brought warm moist air to form summer Arctic stratus clouds, while the latter originated from north central Russia and transported to Barrow that contributed to Arctic winter pollution and the Arctic haze season. They also found that no pollution sources were transported from either the contiguous United States or Europe during the 8-year period.

The climatology of aerosol characteristics in this region and their typical trajectories supports our findings - small (large) cloud-droplet effective radius and high (low) concentration during the spring (summer) when the aerosol concentration is high (low). Although the studies cited here are not directly related to the same study period, we know of no reason to suspect that their results would not hold generally. Certainly more study is needed to investigate the day-to-day and month-to-month variations of aerosol column concentrations at the ARM NSA site for this study period that would enable studies on the relationship between aerosol properties and cloud microphysics.

d. Cloud microphysics

In this section, we compare the summer 2000 results with aircraft in situ measurements from the National Center for Atmospheric Research (NCAR) C-130 (Dong et al. 2001; Lawson et al.

2001) and the University of Washington (UW) Convair-580 (Hobbs et al. 2001) over the SHEBA ship during the FIRE Arctic Clouds Experiment. We also compare with the in situ measurements over the Beaufort Sea observed by the UW Convair C-131A research aircraft in June 1995 (Hobbs and Rangno 1998) and by the NCAR Electra aircraft during the Arctic Stratus Clouds (ASC) experiment in June 1980 (Herman and Curry 1984). Finally, the cloud microphysics observed by the NCAR C-130 aircraft during the Beaufort and Arctic Storms Experiment (BASE) from late September to early October, 1994 is also listed in Table 4 (Pinto et al. 2001).

The aircraft results in Dong et al. (2001) were averaged from 1 or 2 hours of Forward Scattering Spectrometer Probe (FSSP-100) measurements when the aircraft was within a radius of 10 km of the SHEBA ship. In Lawson's study, LWC was measured by a King hot-wire LWC device and N by a FSSP-100. In Hobbs et al. (2001) and Hobbs and Rangno (1998) studies, the r_e and N values were measured by the same probe - FSSP-100, while the LWC values were observed by the Gerber Scientific Particle Volume Monitor-100 (PVM-100) and the King probe, respectively. The cloud microphysical properties in Herman and Curry (1984) and Pinto et al. (2001) studies were measured by the Knollenberg FSSP and FSSP-100, respectively.

Comparing Table 4 with Table 2, we find that in all comparisons, one or two parameters of the surface-derived cloud microphysics agree with the in situ data but not all at the same time. While it is possible that the discrepancies may be due to instrumental or algorithmic uncertainties, they can also arise from the effects of ice crystals in otherwise liquid clouds, cloud vertical structure that is not totally sampled by the aircraft measurements, and different location and year. Although these comparisons using the surface and aircraft data are quite limited, it appears that the surface-retrieved cloud microphysical properties have a certain degree of agreement with the aircraft in situ measurements. No attempt has been made to validate the surface-retrieved cloud microphysics using aircraft observations; rather, we want to know whether the surface results and in situ measurements are roughly the same.

e. Radiative properties

Using a simple radiation mode, Leontyeva and Stamnes (1994) estimated cloud optical depths from ground-based measurements of incoming solar irradiance at Barrow during April-October 1988. The estimations of cloud optical depth were performed for all overcast cloudy conditions based on hourly mean values of incoming and reflected solar irradiances at the surface measured by the PSP pyranometers with the assumptions of plane-parallel and homogenous cloud layers and fixed r_e (=7 μm). The monthly mean τ values during May-August 1988 were 11, 12, 10, and 20, respectively. The mean values during June and July are nearly the same as those in this study (Table 2), while the mean value in May is smaller. In August, τ derived by Leontyeva and Stamnes is much higher than the values of other months in their study and the same month in this study. The difference of technique for estimating τ between the Leontyeva and Stamnes and this study is that our retrieval is performed only for single-layer and overcast low-level stratus clouds after passing 5 specific criteria, while Leontyeva and Stamnes use all periods regardless of cloud characteristics. A slow moving frontal system, for instance, would likely be enough to significantly bias their results away from typical single layer stratus.

The monthly mean surface albedos during May-September 1988, derived from the reflected and incident solar irradiances in Leontyeva and Stamnes's study, are almost the same as those in this study (Table 2), such as a high value (0.8-0.9) in May and a low value (0.15-0.2) during summer. The monthly frequency distributions of R_{sfc} also show a bimodal distribution with peaks at 0.1-0.2 and 0.8-0.9 during the spring (June) and at 0.1-0.2 and 0.6-0.8 during the autumn (September) transition seasons, which is consistent with this study. Curry et al. (2001) also presented the R_{sfc} values derived from the surface-based PSP measurements during the FIRE ACE and SHEBA field experiments and showed that surface albedos in May and late September are the same as those in this study and during the summer (July and early August) are around 0.5. The spring transition season started in late May and ended around late June, and the autumn began in mid August and ended in late September during the FIRE ACE and SHEBA field experiments. It is not surprising to have good agreement in R_{sfc} between the ARM NSA site and SHEBA ship during the spring and autumn seasons because both sites were covered by snow in these two transition seasons. During summer, the difference of R_{sfc} in these two sites is mainly due to the latitude difference where the SHEBA ship was approximately 5-9^{o} north of the ARM NSA site. The ARM NSA site during summer is normally covered by low-albedo tundra surrounded by

open water (Leontyeva and Stamnes 1994), while the SHEBA ship was covered by a mosaic of low-albedo melt ponds interspersed with much higher albedo regions of ice (Curry et al. 2001).

f. Cloud Radiative forcing

Intrieri et al. (2001a) studied an annual cycle of Arctic surface cloud radiative forcing from data obtained during the SHEBA experiment. The definition of CRF in their study is the same as in this study, and the instruments for measuring SW and LW fluxes are the same as those at the ARM NSA site. During the SHEBA experiment, the SW CRFs slowly decreased from 0 to –10 W m^{-2} and LW CRFs remained nearly a constant value of 40 W m^{-2}, resulted in a positive net CRF of ~30-40 W m^{-2} from early May to late June. During late June-early July, the SW CRFs suddenly dropped from –10 to –50 W m^{-2} and LW CRFs slightly increased from about 30 to 45 W m^{-2}, leading to a small negative net CRF (~ -5 W m^{-2}) in one or two weeks. The SW and LW CRFs at the SHEBA ship monotonically increased from –50 to ~0 W m^{-2} and from 45 to 60 W m^{-2}, respectively, from middle July to middle September. This result is similar to the finding in Curry et al. (1996) for 80^{o}N, but much different to this study (Table 2 and Fig. 6). The LW CRFs between the ARM NSA site and SHEBA ship are nearly the same, but the values of negative SW CRF at the ARM NSA are much larger than at the SHEBA ship. Comparing the net CRFs at the ARM NSA site with those at the SHEBA ship, the summer cooling period at the ARM NSA is much longer (2-3 months vs. 1-2 weeks), and the values of negative net CRF are much larger (-100 W m^{-2} vs. -5 W m^{-2}).

It should be noted that the SW and LW fluxes during the cloudy conditions in Intrieri et al. study are for all clouds compared to single-layer and overcast low-level stratus clouds only in this study. To study the difference of CRF between all clouds and low-level stratus clouds, two months of CRFs are calculated for all clouds in May and August at the ARM NSA site and shown in Table 5. The net CRFs of all clouds in these two months are almost the same as those of low-level stratus clouds (Table 2) because most of all clouds are optically thick in these two months as we learned in this study and demonstrated in the Table 2 of Leontyeva and Stamnes (1994). We also notice that this comparison is based on the 5-9^{o} latitude difference between the SHEBA ship (76-80^{o}N) and ARM NSA site (71^{o}N). To further study the impact of surface albedo on the surface radiation budget, we calculate the CRFs of low-level stratus clouds in

August at the ARM NSA site with the fixed R_{sfc}=0.5 for both clear and cloudy periods. As shown in Table 6, the LW CRFs are the same but the SW CRFs are significantly decreased, which results in a small negative net CRF.

g. Summary

The formation, maintenance, and dissipation processes of Arctic stratus clouds are significantly different from the midlatitudes stratus clouds. In the Arctic the dissipative processes that destroy stratus clouds in midlatitudes, such as precipitation, convective heating from the surface, and absorption of solar radiation, are either nonexistent and/or are relatively weak. Despite the scale differences between surface and satellite observations, the limited resolution of the satellite imager pixels, and the low resolution of surface cloud fraction digitization (octas) and surface observer subjectivity, the comparison of cloud fractions between this study and the FIRE ACE and SHEBA experiments shows good agreement. For the cloud microphysics, one or two parameters of the surface-derived cloud microphysics in this study agree with the in situ data but not all at the same time. Although these comparisons using the surface and aircraft data are quite limited, the surface-retrieved cloud microphysical properties in this study agree reasonably well within the range found by aircraft in situ measurements over the Arctic Ocean during other field experiments. The climatology of Arctic aerosol characteristics and their trajectories shows a maximum concentration in winter contributed by anthropogenic sources in northern central Russia and a minimum in summer. This correlates precisely with the seasonal variation of cloud microphysics found in this study. The surface albedos at the SHEBA and the ARM NSA site are similar in May and late September because both sites are snow-covered. Comparing the net CRFs at the ARM NSA site with those at the SHEBA ship, the summer cooling period at the ARM NSA site is much longer (2-3 months vs. 1-2 weeks), and the values of negative net CRF are much larger (-100 W m^{-2} vs. -5 W m^{-2}). The reason leading to the difference of net CRF at two sites is mainly due to much higher surface albedo and solar zenith angle at the SHEBA ship than at the ARM NSA site.

5. Conclusions

A 5-month record of low-level stratus cloud properties (May through September 2000) has been generated to determine the seasonal variation of Arctic stratus cloud macrophysical,

microphysical, and radiative properties at the ARM NSA site, and also to examine the impact of stratus cloud properties on the Arctic surface radiation budget. We have also compared the summer 2000 results with data sets collected elsewhere. From the summer 2000 results and comparisons with other data sets, we are attempting to answer the two scientific questions posed in the introduction:

1) The monthly-averaged cloud properties in this study have been summarized in Table 2. The mean values of total and low-level cloud fractions during the study period are 0.87 and 0.55, and their minimums are in June and maximums are in May and September, respectively. Most of low cloud base heights are around 0.4 km and top heights are 0.8 km except in September where both Z_{base} and Z_{top} values are above 1 km. Both cloud base and top temperatures increase more than 10 K from the spring to the summer. The means of cloud-droplet effective radius and number concentration are around 13 μm and 60 cm^{-3} during the summer, and 8 μm and 220 cm^{-3} during the spring, respectively. The net cloud radiative forcing cools the surface during the summer and warms the surface during the spring and autumn seasons – confirming that Arctic stratus clouds enhance the springtime melting and slow down the autumn freezing of the ice pack compared to having no clouds.
2) The total cloud fractions in this study show good agreement with the satellite and surface results compiled from data collected during the FIRE ACE and SHEBA field experiments in 1998. The cloud microphysics derived from this study, in general, are similar to those collected in past field programs although these comparisons are based on data collected at different locations and different years (the same months). No attempt has been made to validate the surface-based cloud properties in this study using those aircraft and satellite data. Our goal is showing that the summer 2000 results at the ARM NSA site fit within the general context of other data collected in this region. The surface albedos (~0.8) in May and late September are the same as those during the FIRE ACE and SHEBA experiments. In summer the surface albedo at the ARM NSA site (71°N) is around 0.2, which is significantly lower than at the SHEBA ship (~0.5) near 80°N. Comparing the net CRFs at the ARM NSA site with those at the SHEBA ship, the summer cooling period at the ARM NSA site is much longer (2-3 months vs. 1-2 weeks), and the values of negative net CRF are much larger (-100 W m^{-2} vs. -5 W m^{-2}).

The cloud macrophysical and microphysical properties in this study when compared statistically with other similar data sets can approximately represent the climatology of Arctic stratus cloud macrophysical and microphysical properties during May-September period. The ARM NSA site represents reasonably well Arctic land areas and adjacent open ocean regions that transition to low surface albedo and a net negative CRF in summertime. The SHEBA ship represents sea-ice-covered latitudes with larger surface albedo and weaker solar radiation where the net CRF remains weakly positive or neutral during the summer.

The above conclusions are based on the data complied from May to September 2000 at the ARM NSA site, and on comparisons with limited surface, aircraft, and satellite results at different locations and different years. No attempt has been made to give an overall climatology of Arctic stratus clouds, rather, the emphasis here is to provide fundamental statistical information about Arctic stratus cloud properties that are useful for the purpose of evaluating global/climate models. In order to improve the representation of cloud microphysics and the associated heating and other feedbacks in these models, the actual physical processes that lead to cloud formation and maintenance must be understood to the extent that they can be parameterized to ensure that the hydrological cycle in the models faithfully represent what is found in nature. For example, can we use the surface-based observations to explore some of the cloud modeling concepts, such as adiabatic parcel models? Is the different behavior in cloud LWC between the ARM NSA and SGP sites due to the different environmental conditions, or to the greater solar heating at the SGP site, or both? Therefore, the time-dependent frequency distributions of cloud microphysical and radiative properties from the model should be also compared to those derived from data. Ultimately, improved parameterizations can only result from a combined effort that includes long-term observations as we have presented here, cloud resolving models (Krueger, 1988), and single column models (Randall et al. 1996) to test and improve the physical parameterizations of climate models.

Acknowledgments: Data were obtained from the Atmospheric Radiation Measurement (ARM) Program sponsored by the U.S. Department of Energy (DOE) Office of Energy Research, Office of Health and Environmental Research, Environmental Sciences Division. Special thanks for Ms. S. Benson to process the data and for three anonymous reviewers to provide the insightful comments and suggestions. During this study, authors were supported by the ARM program under grant DE-AI02-97ER62341, Dr. Dong was also supported by NASA CERES project under contract NAG-1-2250, and Dr. Mace was also supported by NASA EOS validation project under contract NAG-5-6458.

Appendix

New parameterization

To retrieve the microphysical and radiative properties of single-layer and overcast low-level stratus clouds, D97 used a δ2-stream radiative transfer model in conjunction with ground-based measurements. The retrieval scheme is based on an iterative approach that varies r_e in the radiative transfer calculations until the model-calculated solar transmission matches the measured value. The retrieved cloud properties include the layer-mean cloud-droplet effective radius (r_e) and number concentration (N), broadband shortwave optical depth (τ), and albedos at the top of cloud and atmosphere (R_{cldy}, R_{TOA}) with the derived R_{sfc}. D98 parameterized the retrieved r_e and radiative properties as a function of the cloud LWP, the effective solar transmission (γ), and cosine of the solar zenith angle (μ_0). The retrieved and parameterized cloud microphysical properties have been validated by aircraft in situ measurements in the midlatitudes (Dong et al. 1998; 2002) and in the Arctic region (Dong et al. 2001).

The method to develop the new parameterization is the same as that in D98, at first we retrieve r_e using the D97 technique with the inputs of surface measurements, such as cloud LWP, ΔZ, γ, and R_{sfc}, and then we parameterize r_e as a polynomial function of cloud LWP, γ, μ_0, and R_{sfc}. The D98 parameterization is primarily developed for low R_{sfc} where single-layer, liquid-phase, and daytime cloud conditions exist. The new parameterization, reported here for the first time, is the same as that described by D98 except the impact of R_{sfc} is included. To demonstrate the impact of R_{sfc} on cloud albedo and transmission, Figure A1 is plotted using a 2-stream discrete-ordinate method (Liou 1974). The cloud albedo and transmission only depend on τ for R_{sfc}=0, but they monotonically increase with the increased R_{sfc}. The dependence of cloud albedo and transmission on τ becomes less and less with the increased R_{sfc}. Therefore, cloud albedo and transmission depend on both τ and R_{sfc} for conservative scattering as shown in Fig. A1. However, if clouds absorb appreciably, the influence of R_{sfc} on cloud albedo would depend on the amount of cloud absorption and τ. The effective solar transmission (γ), which is measured the total downward solar flux at the surface, also increases with the increased R_{sfc} due to the multiple reflections of solar radiation between the cloud layer and the highly reflective surface.

To develop the new parameterization, we use 13 cases (~91 hours of data) with the range of R_{sfc} from 0.1 to 0.9 selected from the present study period at the ARM NSA site. The retrieved values of r_e from the D97 method are parameterized as a polynomial function of cloud LWP, γ, μ_0, and R_{sfc} as follows:

$$r_e = 2.49LWP + 10.25(1 - R_{sfc}^3)\gamma - 0.25\mu_0 + 20.28LWP\gamma(1 - R_{sfc}^3) - 3.14LWP\mu_0, \quad \text{(A1)}$$

where the units of LWP and r_e are (100 g m^{-2}) and (μm), respectively. Equation (A1) is similar to (9) of D98 except that R_{sfc} is included. Once r_e is known, N and τ can be estimated

$$N = \frac{3LWP}{4\pi\rho_w r_e^3 \Delta Z}\exp(3\sigma_x^2), \quad \text{(A2)}$$

and

$$\tau = \frac{3lwp}{2r_e\rho_w}. \quad \text{(A3)}$$

The logarithmic width σ_x is set to 0.38 (Miles et al. 2000), and ΔZ is cloud thickness derived from the difference of cloud top and base heights. Fixing σ_x in the scheme does not lead to significant errors in the retrieval values of r_e, while N changes by 15 to 30% as σ_x varies from 0.2 to 0.5 (D97).

The D98 cloud albedo (R_{D98}) and transmission (T_{D98}) were calculated with the inputs of retrieved r_e and N, along with the measured cloud base and top heights using the same radiative transfer model as in the retrieval of r_e and N but with R_{sfc}=0. The resulting values for R_{D98} and T_{D98} are then fit with polynomial function of LWP, r_e, and μ_0:

$$R_{D98} = -0.089 - 0.089r_e - 0.19\mu_0 + 0.405\ln(LWP) - 0.033\ln^2(LWP) + 0.00045r_e^2 + 0.011\ln(LWP)r_e, \quad \text{(A4)}$$

$$T_{D98} = 1.087 + 0.096r_e + 0.153\mu_0 - 0.418\ln(LWP) + 0.034\ln^2(LWP) - 0.0004r_e^2 - 0.012\ln(LWP)r_e, \quad \text{(A5)}$$

where the units of LWP and r_e are (g m^{-2}) and (μm), respectively. The R_{D98} and T_{D98} are nearly the same as bulk cloud top albedo R_{cldy} and measured γ over land and ocean for low R_{sfc}, but not for high R_{sfc}. The R_{cldy}, a result during the retrieval of r_e, has the following relationship with R_{D98}, T_{D98}, and R_{sfc} based on a total of 91 hours of measurements and retrievals:

$$R_{cldy} = R_{D98} + R_{sfc}T_{D98}. \quad \text{(A6)}$$

The R_{cldy} in (A6) will equal to R_{D98} if R_{sfc}=0. The bulk TOA albedo (R_{TOA}), on average, is 82.6% of the R_{cldy} with only a 2% variation around the average value during the 91-hour period. The Root-Mean-Square errors in the parameterizations of r_e and R_{cldy} relative to the retrieved values are similar to those reported in D98, around 11% and 4% (Fig. A2), respectively.

To illustrate the importance of r_e and R_{sfc} to R_{cldy}, Fig. A2 is produced from (A6) for a variety of cloud LWP, r_e and R_{sfc} with a specified μ_0. As Fig. A2 demonstrated, for fixed LWP, R_{cldy} has a significant dependence on both r_e and R_{sfc}. The quantitative dependence of r_e on cloud LWP, γ, and R_{sfc} is also illustrated in Fig. A2 where r_e exhibits a strong positive correlation with γ for a given R_{sfc} and a negative correlation with R_{sfc} for a fixed γ. Most of data points (circles) fall within the lower and upper limits of calculations (lines) from the new parameterizations (A1, A6) as shown in Fig. A2.

REFERENCES

Barrie, L.A., 1986: Arctic air pollution: An overview of current knowledge. *Atmos. Environ.,* **20**, 643-663.

Bigg, E.K., 1980: Comparison of aerosol at four baseline atmospheric monitoring stations. *J. Appl. Meteor.,* **19**, 521-533.

Curry, J.A., W.B. Rossow, D. Randall, and J.L. Schramm, 1996: Overview of Arctic cloud and radiation characteristics. *J. Climate,* **9**, 1731-1764.

Curry, J.A., and Coauthors, 2000: FIRE Arctic Clouds Experiment. *Bull. Amer. Meteor. Soc.,* **81**, 5-29.

Curry, J.A., J.L. Schramm, D.K. Perovich, and J.O. Pinto, 2001: Applications of SHEBA/FIRE data to evaluation of snow/ice albedo parameterizations. *J. Geophys. Res.,* **106***,* 15 345-15 355.

Dong, X., T.P. Ackerman, E.E. Clothiaux, P. Pilewskie, and Y. Han, 1997: Microphysical and radiative properties of stratiform clouds deduced from ground-based measurements. *J. Geophys. Res*., **102**, 23 829-23 843.

Dong, X., T.P. Ackerman, and E.E. Clothiaux, 1998: Parameterizations of microphysical and shortwave radiative properties of boundary layer stratus from ground-based measurements. *J. Geophys. Res.,* **103**, 31 681-31 693.

Dong, X., P. Minnis, T.P. Ackerman, E.E. Clothiaux, G.G. Mace, C.N. Long, and J.C. Liljegren, 2000: A 25-month database of stratus cloud properties generated from ground-based measurements at the ARM SGP site. *J. Geophys. Res*., **105**, 4529-4538.

Dong, X., G.G. Mace, P. Minnis, and D.F. Young, 2001: Arctic stratus cloud properties and their effect on the surface radiation budget: selected cases from FIRE ACE. *J. Geophys. Res*., **106**, 15 297-15 312.

Dong, X., P. Minnis, G.G. Mace, W.L. Smith Jr, M. Poellot, and R.T. Marchand, 2002: Comparison of stratus cloud properties deduced from surface, GOES, and aircraft data during the March 2000 ARM cloud IOP. Accepted by *J. Atmos. Sci.*

Gates, W.L., 1992: AMIP: The Atmospheric Model Intercomparison Project. *Bull. Amer. Meteor. Soc*., **73**, 1962-1970.

Harris, J.M., and J.D.W. Kahl, 1994: Analysis of 10-day isentropic flow patterns for Barrow,

Alaska: 1985-1992. *J. Geophys. Res.,* **99***,* 25 845-25 855.

Harrison, E.F., P. Minnis, B.R. Barkstrom, V. Ramanathan, R.D. Cess, and G.G. Gibson, 1990: Seasonal variation of cloud radiative forcing derived from the Earth Radiation Budget Experiment. *J. Geophys. Res.,* **95**, 18 687-18 703.

Hartmann, D.L., M.E. Ockert-bell, and M.L. Michelsen, 1992: The effect of cloud type on Earth's energy balance: Global analysis. *J. Climate*, **5**, 1281-1304.

Herman, G.F., and R. Goody, 1976: Formation and persistence of summertime Arctic stratus clouds. *J. Atmos. Sci.,* **33**. 1537-1553.

Herman, G.F., and J.A. Curry, 1984: Observational and theoretical studies of solar radiation in Arctic stratus clouds. *J. Climate and Appl. Meteor.*, **23**, 5-24.

Hobbs, P.V., and A.L. Rangno, 1998: Microstructures of low and middle-level clouds over the Beaufort Sea. *Quart. J. Roy. Meteor. Soc.*, **124**, 2035-2071.

Hobbs, P.V., A.L. Rangno, M.D. Shupe, and T. Uttal, 2001: Airborne studies of cloud structures over the Arctic Ocean and comparisons with retrievals from ship-based remote sensing instruments. *J. Geophys. Res.,* **106**, 15 029-15 044..

Intrieri, J.M., C.W. Fairall, M.D. Shupe, P.O.G. Persson, E.L. Andreas, P.S. Guest, and R.E. Moritz, 2001a: An annual cycle of Arctic surface cloud forcing at SHEBA. *J. Geophys. Res.,* in press.

Intrieri, J.M., M.D. Shupe, T. Uttal, and B.J. McCarty, 2001b: An annual cycle of Arctic cloud characteristics observed by radar and lidar at SHBEA. *J. Geophys. Res.,* in press.

Kato, S., T.P. Ackerman, E.E. Clothiaux, J.H. Mather, G.G. Mace, M.L. Wesely, F. Murcray, and J. Michalsky, 2001: Uncertainties in modeled and measured clear-sky surface shortwave irradiance. *J. Geophys. Res.,* **102**, 25 881-25898.

Krueger, S.K., 1988: Numerical simulation of tropical cumulus clouds and their interaction with the subcloud layer. *J. Atmos. Sci.,* **45**, 2221-2250.

Lawson, R.P., B.A. Baker, C.G. Schmitt, and T.L. Jensen, 2001: An overview of microphysical properties and Arctic clouds observed in May and July 1998 during FIRE ACE. *J. Geophys. Res.,* **106**, 14 989-15 014.

Leontyeva, E., and K. Stamnes, 1994: Estimates of cloud optical thickness from ground-based measurements of incoming solar radiation in the Arctic. *J. Climate*, **7**, 566-578.

Liljegren, J. C., E.E. Clothiaux, G.G. Mace, S. Kato, and X. Dong, 2001: A new retrieval for cloud liquid water path using a ground-based microwave radiometer and measurements of cloud temperature. *J. Geophys. Res*., **106**, 14 485-14 500.

Lilly, D.K., 1968: Models of cloud-topped mixed layer under a strong inversion. *Quart. J. Roy. Meteor. Soc.,* **94,** 292-309.

Liou, K.N., 1974: Analytic two-stream and four-stream solutions for radiative transfer. *J. Atmos. Sci.,* **31**, 1473-1475.

Long, C.N., and T.P. Ackerman, 2000: Identification of clear skies from broadband pyranometer measurements and calculation of downwelling shortwave cloud effects. *J. Geophys. Res., **105**,* 15 609-15 626.

Maslanik, J.A., J. Key, C.W. Fowler, T. Nguyen, and X. Wang, 2001: Spatial and temporal variability of satellite-derived cloud and surface characteristics during FIRE-ACE. *J. Geophys. Res.,* **106***,* 15 223-15 249.

Miles, N.L., J. Verlinde, and E.E. Clothiaux, 2000: Cloud-droplet size distributions in low-level stratiform clouds. *J. Atmos. Sci.,* **57**, 295-311.

Minnis P., V. Chakrapani, D.R. Doelling, L. Ngugen, R. Palikonda, D.A. Spangenberg, T. Uttal, R.F. Arduini, and M.D. Shupe, 2001: Cloud coverage and height during FIRE ACE derived from AVHRR data. *J. Geophys. Res.,* **106**, 15 215-15 232.

Mitchell, J.F.B., and W.J. Ingram, 1992: Carbon dioxide and climate: Mechanisms of changes in cloud. *J. Climate*., **5**, 5-21.

Moran, K.P., B.E. Martner, M.J. Post, R.A. Kropfli, D.C. Welsh, and K.B. Widener, 1998: An unattended cloud-profiling radar for use in climate research. *Bull. Amer. Meteor. Soc*., **79**, 443-455.

Paluch, I.R., and D.H. Lenschow, 1991: Stratiform cloud formation in the marine boundary layer. *J. Atmos. Sci.,* **48**, 2141-2158.

Perovich, D.K., and Coauthors, 1999: Year on ice gives climate insights. *Eos. Trans., Amer. Geophs. Union,* **80**, 481.

Pinto, J.O., J.A. Curry, and J.M. Intrieri: 2001: Cloud-aerosol interactions during the autumn over Beaufort Sea. *J. Geophys. Res.,* **106**, 15 077-15 097.

Randall D., K.-M. Xu, R.J.C. Somerville, and S. Iacobellis, 1996: Single-column models and cloud ensemble models as links between observations and climate models. *J. Climate*, **9**,

1683-1697.

Randall, D., and Coauthors, 1998: Status of and outlook for large-scale modeling of atmospheric -ice-ocean interactions in the Arctic. *Bull. Amer. Meteor. Soc*., **78**, 197-219.

Ramanathan, V., R.D. Cess, E.F. Harrison, P. Minnis, B.R. Barkstrom, E. Ahmad, and D. Hartmann, 1989: Cloud-radiative forcing and climate: Results from the Earth Radiation Budget Experiment. *Science*, **243**, 57-63.

Stamnes, K., R.G. Ellingson, J.A. Curry, J.E. Walsh, and B.D. Zak, 1999: Review of science issues, development strategy, and status for the ARM North Slope of Alaska-Adjacent Arctic Ocean climate research site. *J. Climate,* **12**, 46-63.

Stokes, G.M., and S.E. Schwartz, 1994: The Atmospheric Radiation Measurement (ARM) program: Programmatic background and design of the cloud and radiation testbed. *Bull. Amer. Meteor. Soc*., **8**, 1251-1256.

Stone, R.S., 1997: Variations in western arctic temperature in response to cloud radiative and synoptic-scale influence. *J. Geophys. Res.*, **102**, 21 769-21 776.

Tao, X., J.E. Walsh, and W.L. Chapman, 1996: An assessment of global climate simulations of Arctic air temperatures. *J. Climate*, **9**, 1060-1076.

Tsay, S.-C., and K. Jayaweera, 1984: Physical characteristics of Arctic stratus clouds. *J. Climate and Appl. Meteor.*, **23**, 584-596.

Westwater, E.R., Y. Han, M.D. Shupe, and S.Y. Matrosov, 2001: Analysis of integrated cloud liquid and precipitable water vapor retrievals from microwave radiometers during SHEBA. *J. Geophys. Res.,* in press.

Wetherald, R.T., and S. Manabe, 1988: Cloud feedback processes in general circulation model. *J.*

Atmos. Sci., **45**, 1397-1415.

Figure Captions

Fig. 1. The 10-day means (standard deviations) are simply the averages of total and low cloud occurrences for all cloudy conditions, and the averages of the selected samples (5-min) using 5 criteria for cloud base and top heights/temperatures within a 10-day period. The cloud base and top heights derived from the radar and ceilometer measurements, respectively, and cloud base and top temperatures from the ARM NSA rawinsonde sounding (~local noon) using the ceilometer and radar derived cloud base and top heights.

Fig. 2. Frequency distributions of cloud macrophysical and microphysical properties from the 5-month data during May-September 2000 at the ARM NSA site.

Fig. 3. 10-day averages and standard deviations of cloud parameters based on the selected samples (5-min) using 5 criteria within a 10-day period. Cloud LWP retrieved from microwave radiometer measured brightness temperature, cloud LWC derived from the ratio of LWP to ΔZ, and cloud-droplet effective radius and number concentration calculated from the newly developed parameterization.

Fig. 4. 10-day averages and standard deviations of cloud optical depth, cloud and TOA albedos calculated from the newly developed parameterization, as well as solar transmission and surface albedo derived from the PSP pyranometer measurements based on the selected samples (5-min) using 5 criteria within a 10-day period.

Fig. 5. Frequency distributions of cloud radiative properties from the 5-month data (~300 hours and 3600 samples) during May-September 2000 at the ARM NSA site.

Fig. 6. The 10-day means of clear-sky net LW and SW fluxes are calculated from pyrgeometer measurements and inferred SW flux, respectively, for the daytime (μ_0>0.2) during the 10-day period. The 10-day means of cloudy net SW and LW fluxes are for the selected samples using 5 criteria. The 10-day SW (LW) CRF is the difference between cloudy and clear-sky net SW (LW) 10-day means, and the 10-day net CRF is the summation of SW and LW CRFs (the values of CRF are negative for cooling and positive for warming of the surface) from May to September 2000 at the ARM NSA site.

Fig. A1. Cloud albedo and transmission are calculated by a 2-stream discrete-ordinate method to study the impact of surface albedo on cloud albedo and transmission. The effective solar transmission (γ) is the total downward solar flux at the surface.

Fig. A2. The lines represent the calculated cloud top albedo from (A6) and effective radius from (A1), and the circles represent the data (~91 hours). The calculated cloud effective radius and albedo (Para) are also compared with the retrieved cloud properties (Retr) in the right column.

TABLE Captions

TABLE 1. Summary of surface instruments at the ARM NSA site

TABLE 2. Monthly Mean Values of Cloud Properties at the ARM NSA site.

TABLE 3. Comparison of monthly-averaged total cloud fractions at the ARM NSA site and SHEBA ship

TABLE 4. Comparison of cloud microphysics at the ARM NSA site and SHEBA ship

TABLE 5. Monthly mean CRFs for all cloud conditions at the ARM NSA site

TABLE 6. Monthly mean CRFs for R_{sfc}=0.5 (both clear and cloudy sky) in August at the ARM NSA site

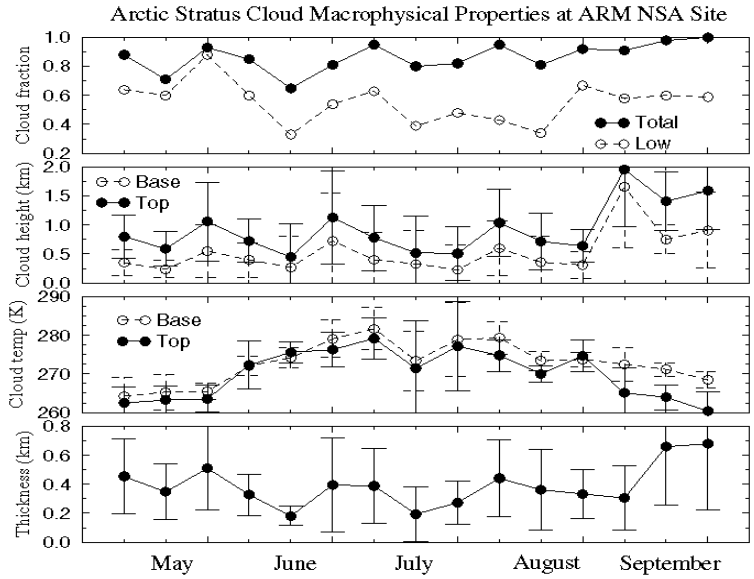

Fig. 1. The 10-day means (standard deviations) are simply the averages of total and low cloud occurrences for all cloudy conditions, and the averages of the selected samples (5-min) using 5 criteria for cloud base and top heights/temperatures within a 10-day period. The cloud base and top heights derived from the radar and ceilometer measurements, respectively, and cloud base and top temperatures from the ARM NSA rawinsonde sounding (~local noon) using the ceilometer and radar derived cloud base and top heights.

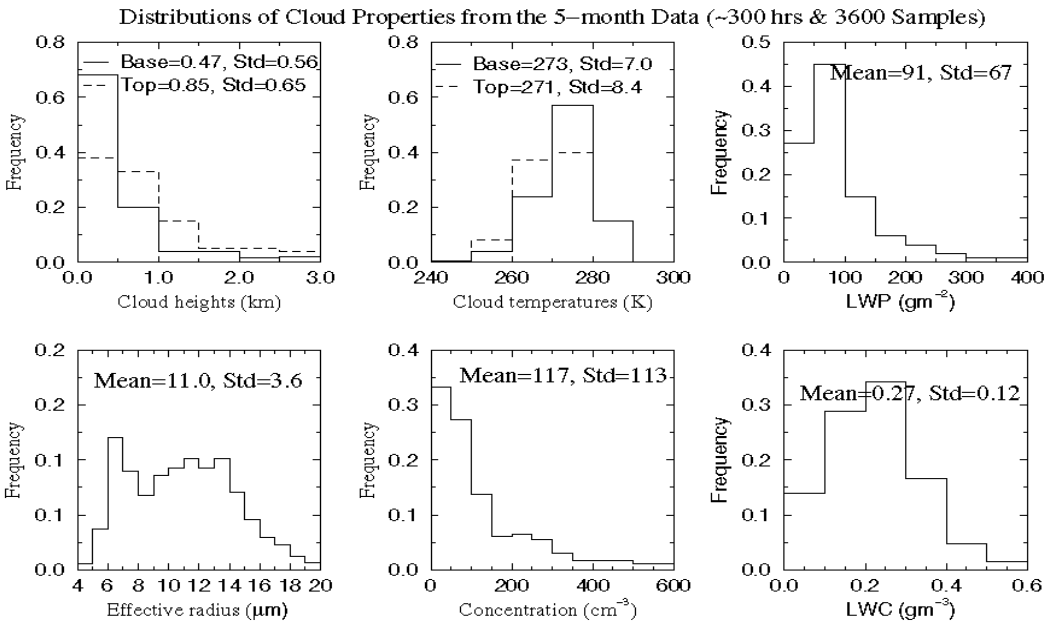

Fig. 2. Frequency distributions of cloud macrophysical and microphysical properties from the 5-month data during May-September 2000 at the ARM NSA site.

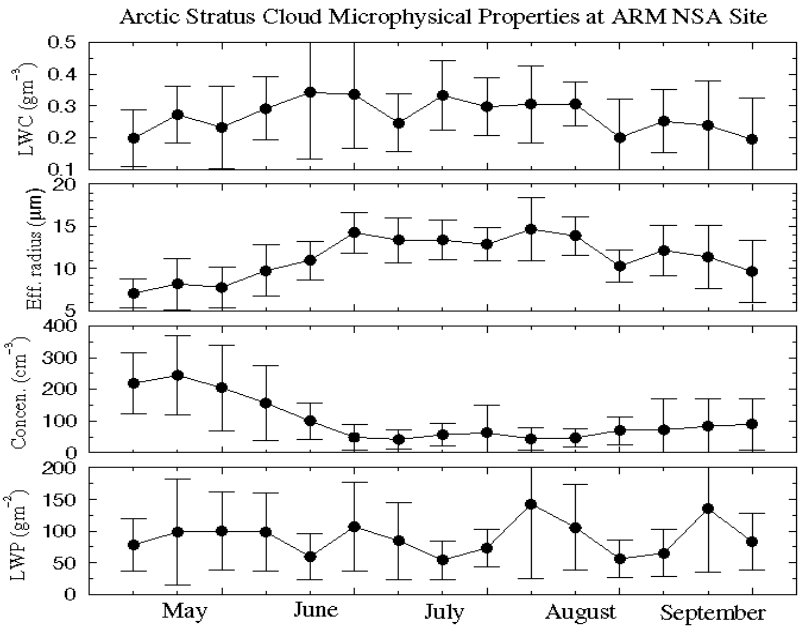

Fig. 3. 10-day averages and standard deviations of cloud parameters based on the selected samples (5-min) using 5 criteria within a 10-day period. Cloud LWP retrieved from microwave radiometer measured brightness temperature, cloud LWC derived from the ratio of LWP to ΔZ, and cloud-droplet effective radius and number concentration calculated from the newly developed parameterization.

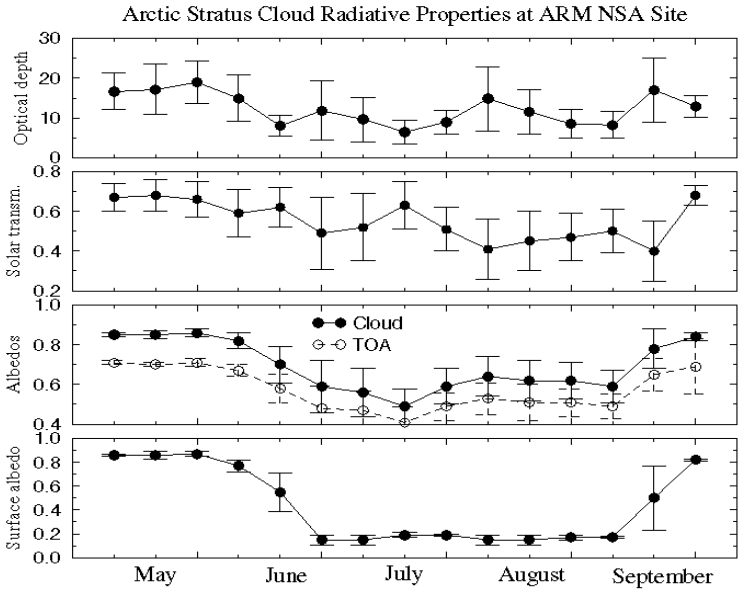

Fig. 4. 10-day averages and standard deviations of cloud optical depth, cloud and TOA albedos calculated from the newly developed parameterization, as well as solar transmission and surface albedo derived from the PSP pyranometer measurements based on the selected samples (5-min) using 5 criteria within a 10-day period.

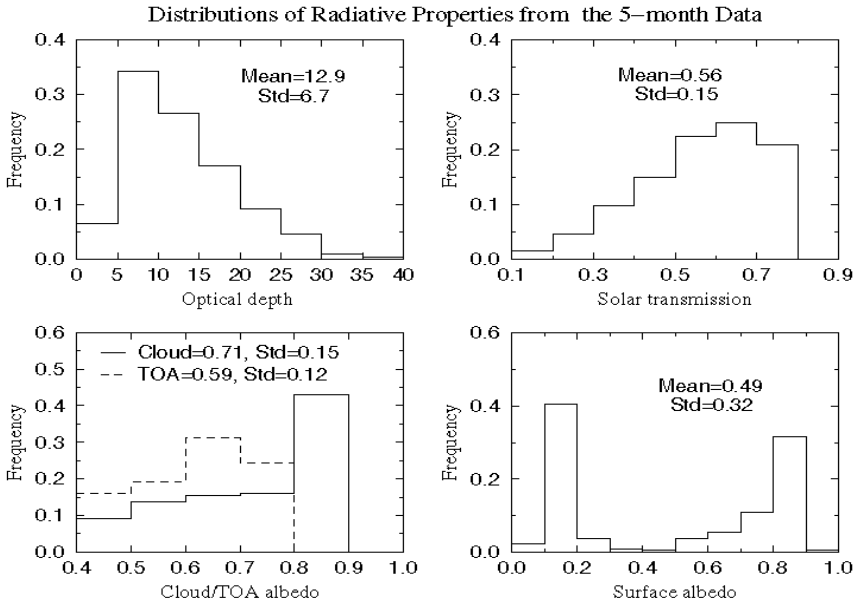

Fig. 5. Frequency distributions of cloud radiative properties from the 5-month data (~300 hours and 3600 samples) during May-September 2000 at the ARM NSA site.

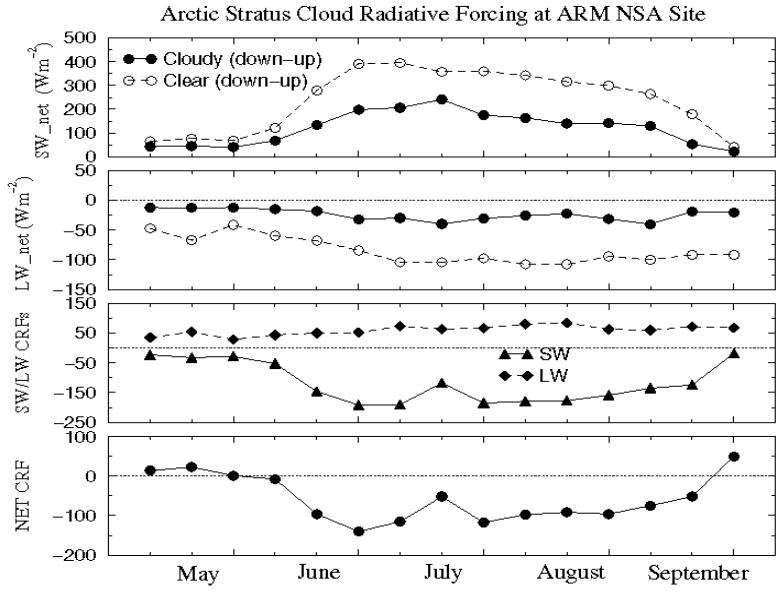

Fig. 6. The 10-day means of clear-sky net LW and SW fluxes are calculated from pyrgeometer measurements and inferred SW flux, respectively, for the daytime (μ_0>0.2) during the 10-day period. The 10-day means of cloudy net SW and LW fluxes are for the selected samples using 5 criteria. The 10-day SW (LW) CRF is the difference between cloudy and clear-sky net SW (LW) 10-day means, and the 10-day net CRF is the summation of SW and LW CRFs (the values of CRF are negative for cooling and positive for warming of the surface) from May to September 2000 at the ARM NSA site.

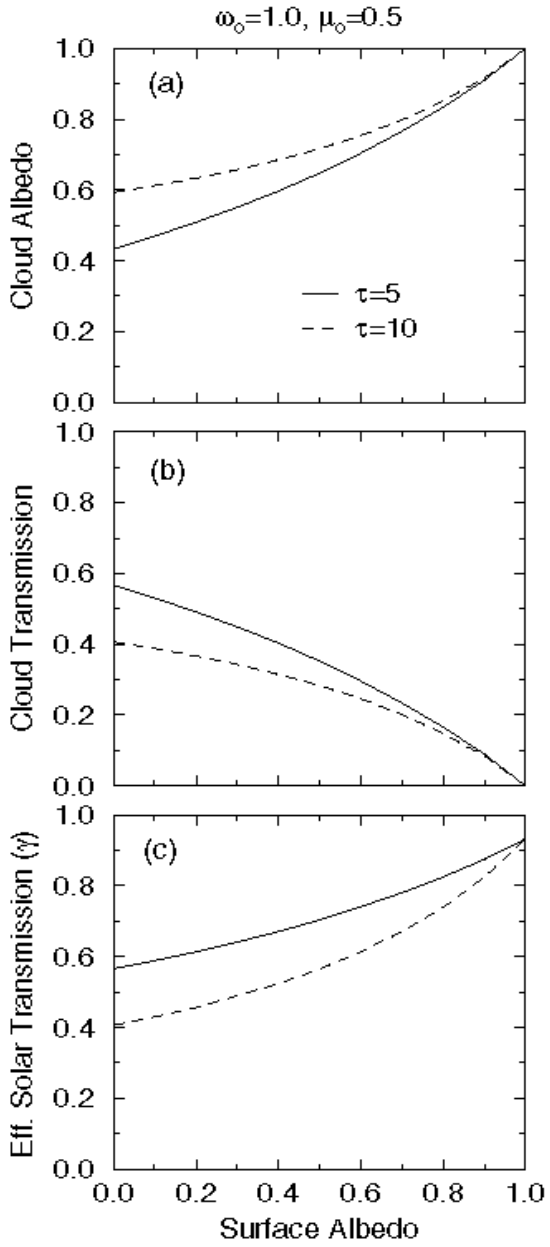

Fig. A1. Cloud albedo and transmission are calculated by a 2-stream discrete-ordinate method to study the impact of surface albedo on cloud albedo and transmission. The effective solar transmission (γ) is the total downward solar flux at the surface.

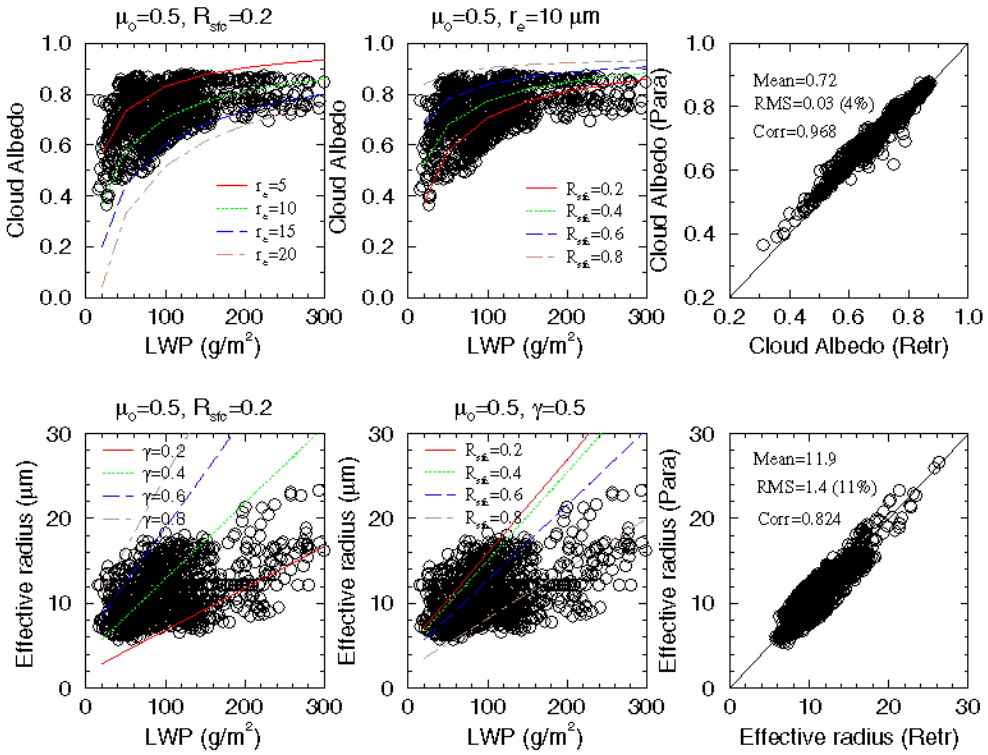

Fig. A2. The lines represent the calculated cloud top albedo from (A6) and effective radius from (A1), and the circles represent the data (~91 hours). The calculated cloud effective radius and albedo (Para) are also compared with the retrieved cloud properties (Retr) in the right column.

TABLE 1. Summary of surface instruments at the ARM NSA site

Instrument	Temporal resolution (s)	Vertical resolution (m)	Range (km)	Observed/derived cloud parameters
Cloud radar	10	45	up to 20	Cloud heights, profiles of radar reflectivity, Doppler velocity and spectral width
Ceilometer	30	7.6	up to 7.5	Cloud base height
Rawinsonde	1/day	5	up to 25	Profiles of pressure, temperature, and relative humidity
Microwave radiometer	300	N/A	N/A	Column integrated liquid water and water vapor
PSP Pyranometer	60	N/A	N/A	Downward/upward broadband SW flux
PIR Pyrgeometer	60	N/A	N/A	Downward/upward broadband LW flux

TABLE 2. Monthly Mean Values of Cloud Properties at the ARM NSA site

	May	June	July	Aug.	Sept.
C_{tot}	0.83	0.77	0.86	0.89	0.96
C_{low}	0.69	0.47	0.50	0.48	0.59
Z_{base}, km	0.389	0.431	0.297	0.393	1.059
Z_{top}, km	0.830	0.736	0.591	0.762	1.608
T_{base}, K	265.1	274.1	278.3	274.9	271.3
T_{top}, K	263.2	273.9	276.1	272.9	264.0
Lwp, gm^{-2}	94.1	89.6	74.8	94.6	107.4
Lwc, gm^{-3}	0.237	0.308	0.291	0.263	0.237
r_e, μm	7.77	11.03	13.39	12.6	11.45
N, cm^{-3}	222.4	121	53.9	56.2	81.4
τ	17.7	12.5	8.6	10.9	13.8
γ	0.688	0.576	0.544	0.448	0.465
R_{cldy}	0.852	0.739	0.553	0.623	0.729
R_{TOA}	0.703	0.611	0.457	0.514	0.602
R_{sfc}	0.860	0.589	0.172	0.157	0.432
SW_{clear}	70.0	263.1	370.3	319.2	161.3
SW_{cloud}	42.4	110.8	203.7	145.3	74.6
LW_{clear}	-51.7	-70.5	-101.8	-102.9	-94.1
LW_{cloud}	-12.1	-19.0	-32.4	-26.7	-26.2
CRF_{SW}	-27.6	-152.3	-166.6	-173.9	-86.7
CRF_{LW}	39.6	51.5	69.4	76.2	67.9
CRF_{NET}	12.0	-100.8	-97.2	-97.7	-18.8

TABLE 3. Comparison of monthly-averaged total cloud fractions at the ARM NSA site and SHEBA ship

Location	Observation	Source	May	June	July	Aug.	Sept.
ARM	Sfc radar/lidar	This study	0.83	0.77	0.86	0.89	0.96
SHEBA	Sfc radar/lidar	Intrieri et al. 2001b	0.88	0.87	0.94	0.92	0.97
SHEBA	Sfc observation	Minnis et al. 2001	0.76	0.76	0.87		
SHEBA	AVHRR	Minnis et al. 2001	0.71	0.75	0.84		
SHEBA	AVHRR	Maslanik et al. 2001	0.93	0.88	0.78		
SHEBA	ISCCP	Minnis et al. 2001	0.59	0.55	0.57		

TABLE 4. Summary of aircraft in situ measurements collected over the Arctic region during other field experiments

Observation	Date (MM-DD-YY)	Time (UTC=LT+10)	Latitude (N)	Longitude (W)	r_e (μm)	N (cm^{-3})	LWC ($g\ m^{-3}$)
NCAR C-130[1]	5-04-98	23:15-24:15	76.0	165.4	7.9	206	0.32
NCAR C-130[1]	5-15-98	21:50-24:00	76.3	165.3	8.7	59	0.16
NCAR C-130[2]	5-18-98	22:08-22:11	76.0	165.2	N.A.	50-150	0.1-0.2
NCAR C-130[1]	5-27-98	22:35-24:20	76.6	168.0	9.1	43	0.09
UW Convair-580	5-29-98	22:11-22:42	76.7	168.1	7.3-15.3	7-50	0.01-0.09
UW Convair-580	6-03-98	21:28-21:29	76.8	167.6	5.5-7.7	65-70	0.03-0.06
UW C-131A	6-06-95	N.A.	70.5	145.0	5.3-8.4	20-225	0.19-0.30
UW C-131A	6-14-95	N.A.	73.0	147.0	7.4-11.7	63-102	0.16-0.49
NCAR Electra	6-20-80	N.A.	72.0-73.8	157.3-159.3	6.5-7.9	178-244	0.15-0.20
NCAR Electra	6-28-80	N.A.	77.1-78.0	154.3-155.1	6.2-7.1	220-365	0.15-0.35
NCAR C-130[2]	7-21-98	22:53-23:24	78.3	165.7	N.A.	30-60	0.05-0.20
NCAR C-130[2]	7-29-98	22:36-23:05	78.5	163.2	N.A.	0-80	0-0.30
NCAR C-130[3]	9-21-94	20:46	73.0-73.1	134.9	8.5	59	N.A.
NCAR C-130[3]	10-12-94	21:30-23:56	70.3-72.1	134.8-137.0	9.0-10.5	62-96	N.A.

NCAR C-130[1], NCAR C130[2], and NCAR C-130[3] are from the sources of Dong et al. 2001, Lawson et al. 2001, and Pinto et al. 2001, respectively.

TABLE 5. Monthly mean CRFs for all cloud conditions at the ARM NSA site

Month	SW_{cloud}	LW_{cloud}	CRF_{SW}	CRF_{LW}	CRF_{NET}
May	55.1	-23.0	-15.0	28.7	13.7
August	143.7	-30.4	-175.5	72.5	-103.0

TABLE 6. Monthly mean CRFs for R_{sfc}=0.5 (both clear and cloudy sky) in August at the ARM NSA site

SW_{clear}	SW_{cloud}	LW_{clear}	LW_{cloud}	CRF_{SW}	CRF_{LW}	CRF_{NET}
189.6	87.0	-102.6	-26.7	-102.6	76.2	-26.4